CONFINEMENT PHYSICS STUDY IN A SMALL LOW-ASPECT-RATIO HELICAL DEVICE CHS

S. OKAMURA, K. MATSUOKA, R. AKIYAMA, D. S. DARROW[1], A. EJIRI[2],
A. FUJISAWA, M. FUJIWARA, M. GOTO, K. IDA, H. IDEI, H. IGUCHI, N. INOUE,
M. ISOBE, K. ITOH, S. KADO, K. KHLOPENKOV[3], T. KONDO[3], S. KUBO,
A. LAZAROS[4], S. LEE, G. MATSUNAGA[5], T. MINAMI, S. MORITA, S. MURAKAMI,
N. NAKAJIMA, N. NIKAI[5], S. NISHIMURA, I. NOMURA, S. OHDACHI, K. OHKUNI[5],
M. OSAKABE, R. PAVLICHENKO[3], B. PETERSON, R. SAKAMOTO, H. SANUKI,
M. SASAO, A. SHIMIZU[5], Y. SHIRAI[3], S. SUDO, S. TAKAGI[5], C. TAKAHASHI,
S. TAKAYAMA[3], M. TAKECHI[5], K. TANAKA, K. TOI, K. YAMAZAKI,
M. YOKOYAMA, Y. YOSHIMURA, T. WATARI

National Institute for Fusion Science,
Toki 509-5292,
Japan

Abstract

The configuration parameter of the plasma position relative to the center of the helical coil winding is very effective one for controlling the MHD stability and the trapped particle confinement in Heliotron/Torsatron systems. But these two characteristics are contradictory to each other in this parameter. The inward shifted configuration is favorable for the drift-orbit-optimization but it is predicted unstable with the Mercier criterion. Various physics problems, such as electric field structure, plasma rotation and MHD phenomena, have been studied in CHS with a compromising intermediate position. With this standard configuration, CHS has supplied experimental results for understanding general toroidal confinement physics and low-aspect-ratio helical systems. In the recent experiments, it was found that the wide range of inward shifted configurations gives stable plasma discharges without any restriction to the special pressure profile. Such enhanced range of operation made it possible to study experimentally the drift-orbit-optimized configuration in the Heliotron/Torsatron systems. The effect of configuration improvement was studied with plasmas in a low collisionality regime.

1. INTRODUCTION

CHS (Compact Helical System) is a small low-aspect-ratio Heliotron/Torsatron device ($A_p \sim 5$) [1]. Since its construction at ten years ago, various plasma physics experiments have been conducted. The main objective was to confirm the advantage of low-aspect-ratio design of Heliotron/Torsatron system and to supply the experimental database for the next generation helical system LHD [2]. A large part of the scientific achievement in helical system research that supported the decision of constructing LHD came from the Heliotron-E experiments. Since there was a large difference in the aspect ratio between two machines ($A_p \sim 11$ for H-E and $A_p \sim 6.5$ for LHD), the scientific experience of the CHS experiment was very important to proceed to LHD. The dataset of global confinement of CHS has been incorporated into the world-wide stellarator scaling study [3] and it confirmed that the confinement capability of CHS is on the general scaling line of global confinement for helical systems. A low-aspect-ratio design of a Heliotron/Torsatron system generally gives a higher MHD stability limit. CHS achieved the highest beta value among helical systems [4] and demonstrated the possibility of realizing the stable discharge with a necessary beta for helical reactor designs.

---

1) Princeton Plasma Physics Laboratory, Princeton, N. J., U.S.A.
2) The Graduate School of Science, Tokyo Univ., Tokyo 113-0033, Japan
3) The Graduate Univ. for Advanced Studies, Toki 509-5292, Japan
4) National Technical University, Athens, Greece
5) Dep. of Energy Eng. Science, Nagoya Univ., Nagoya 464-8603, Japan

The compactness of the device also benefits to practical aspects of the experiments. It is possible to have a minimum requisite size of minor radius (a ~ 0.2 m) with a relatively small machine size (R = 1 m). This size of minor radius is necessary to clearly separate the core plasma confinement from the various physical processes in the plasma edge region. The advantage of a small size device is especially apparent when a new topic of physical research is planned. The preparation of hardware can be done quickly and at a relatively small cost. Typical examples are new diagnostic tools which have been installed in CHS. They opened new area of physics research in helical systems : the HIBP (heavy ion beam probe) for the electric field study [5], the TVCXS (charge exchange spectroscopy with CCD camera) for the plasma rotation and electric field study [6] and the TESPEL (tracer-encapsulated solid pellet injection) for precise transport study with the impurity injection [7]. Machine operation is flexible for a small size device. The H-mode was studied in the discharges with inductive current which was produced by swinging the poloidal field [8]. The dynamic plasma position control for high beta plasma was also demonstrated [4].

The flexibility of the magnetic field configuration control of CHS enables the optimization study of the magnetic field structure. Although the range of configuration space is limited, the optimization for the drift orbits of deeply trapped particles is possible in the experiment. The essential problem for such an optimization in Heliotron/Torsatron systems is the contradiction of drift orbit optimization and MHD stability. In CHS, the stability of discharges, which is more stable than the limit from the Mercier criterion, gives a much wider configuration space and enables the drift-orbit-optimization study. The effect of higher harmonic ripples in the vicinity of the magnetic axis is clarified in the experiments in the low collisionality regime.

2. MAGNETIC CONFIGURATION OF CHS DEVICE

In Heliotron/Torsatron configurations, a considerable amount of deeply trapped particles in the helical ripples do not escape directly from the confinement region. They drift around following the helical structure of the magnetic field. But such drift orbits and the magnetic surfaces do not always coincide and the deviation of trapped particle orbits from the magnetic surfaces causes the ripple transport processes for low collisionality plasmas. This problem depends on the structure of helical windings. CHS has two helical windings ($l = 2$) with eight toroidal periods (m = 8). These helical coils produce the vacuum rotational transform $\iota = 0.3$ at the center and 1.0 at the boundary. A large pitch modulation of the helical winding ($\alpha^* = 0.3$) is adopted for the CHS device as shown by the winding law of the helical coils given by Eq. (1).

$$\theta = N \phi + \alpha^* \sin(N \phi), \ \ N = m/l, \tag{1}$$

where θ is the toroidal and ϕ is the poloidal angle, respectively. A pitch modulation gives two opposite effects depending on its sign. A negative sign enhances the helical ripples in the inboard side of torus which gives better coincidence of drift orbits to magnetic surfaces. But such a modification of the helical winding reduces the size of the last closed magnetic surface (LCMS). Since the most important subject of CHS was to realize a low-aspect-ratio helical device, a positive number of α^* was selected. From this point of view, CHS has a negatively optimized magnetic field configuration for trapped particle orbits.

Even with a given helical coil structure, the characteristics of the magnetic field configuration can be largely varied with poloidal field control. CHS has three sets of poloidal coils which make it possible to control three free parameters in poloidal field (vertical field, quadrupole field, ...). Because the drift orbits of deeply trapped particles are determined by the structure of the magnetic field strength, they are much less sensitive to the vertical field settings than the configuration of magnetic surfaces. Therefore, it is possible to coincide approximately the magnetic surfaces and the drift orbits by controlling the magnetic surface positions with the poloidal field. In CHS, such a configuration can be obtained by strongly shifting the magnetic surfaces to the inboard side of the torus.

Several magnetic surface characteristics which are important for confinement studies are shown in Fig. 1 as a function of the magnetic axis position R_{ax} [1]. The plasma volume is maximum at R_{ax} = 98 cm which is supposed to be the standard configuration from the viewpoint of making a fat plasma in a small device. The minimum aspect ratio 4.5 is obtained at the same position. The magnetic well is formed in the central region of a vacuum field when R_{ax} > 95 cm. The edge region is stabilized by the magnetic shear. The magnetic well is also increased by the Shafranov shift of magnetic axis for finite beta plasmas. The radius of magnetic well region is plotted in Fig. 1 for both vacuum field and the equilibrium with 1 % average beta. The profile of rotational transform varies depending on R_{ax} parameter. The magnetic shear parameter is largest at R_{ax} = 96 cm and decreases for both the outward shift and the inward shift of magnetic axis.
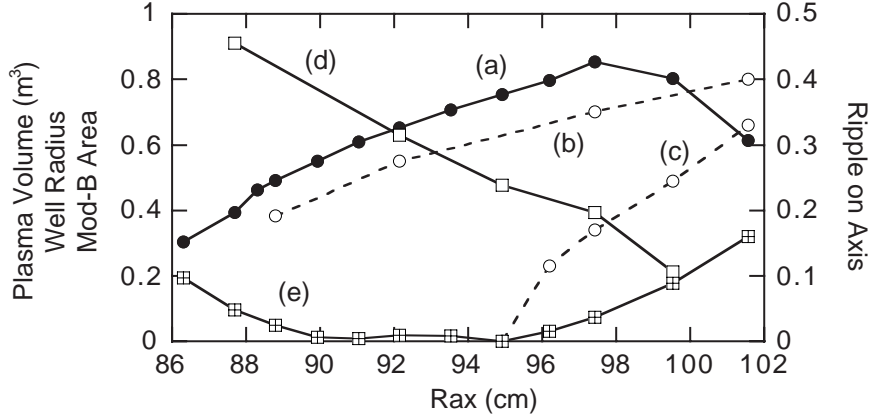

FIG. 1. *Plasma volume (a), normalized radius of magnetic well region for 1 % beta (b) and for 0 % beta (c), relative area of closed Mod-B minimum contour (d), field ripple on magnetic axis (e), as a function of magnetic axis position R_{ax}.*

Most of magnetic axis positions in Fig. 1 are smaller than the major radius of helical coil winding (R = 1 m). It is because of the low aspect ratio characteristics of CHS and the positive pitch modulation of the helical coils. For the standard and inward shifted configurations (R_{ax} < 97 cm), the LCMS is determined by the inboard side of the vacuum vessel wall working as eight symmetric limiters. For the outward shifted configuration, the LCMS is given by the magnetic separatrix.

Drift orbits of deeply trapped particles are approximately illustrated using the Mod-B minimum plots which are contour plots of minimum magnetic field strength along the field line within one helical period. A relative area of the largest Mod-B minimum contour line enclosed by the LCMS is plotted also in Fig. 1. R_{ax} = 87.7 cm gives the best configuration from this point of view while sacrificing plasma volume and the magnetic well. The field ripple on the magnetic axis is also important for the neoclassical heat transport and the parallel viscosity of the plasma rotation. It comes from the two effects of both the helical excursion of the magnetic axis (toroidal effect) and the variation of the distance between the helical coils and the magnetic axis (helical effect). The dependence is shown in Fig. 1.

A large portion of the discharges in CHS have been produced with R_{ax} = 92.1, or 94.9 cm since these configurations gave best performance for both NBI and ECH plasmas in CHS. Such range of magnetic axis position is a standard selection of Heliotron/Torsatron systems to compromise both the MHD stability and trapped particle orbits. This paper describes the experimental results to compare discharges in these standard configurations and more inward shifted configu-

---

[1] Rax is defined as the major radius of a magnetic axis at the vertically elongated toroidal cross section in the vacuum field. It is an operational parameter which reflects the setting of currents in helical and poloidal coils. It does not give the real position of the magnetic axis for a finite beta equilibrium.

rations which gives the drift-orbit-optimization for Heliotron/Torsatron systems.

3. CONFINEMENT CHARACTERISTICS IN STANDARD CONFIGURATION

The database of CHS global confinement time which was incorporated in the international stellarator scaling study (ISS-95) [3] was taken from the discharges with standard configurations (R_{ax} = 92.1 or 94.9 cm). For this study, because the collisionality of most discharges were in the collisional or plateau regime, the characteristics of trapped particle orbits did not have a large effect. More important aspects are anomalous transport and the engineering feasibility of efficient plasma heating. By contributing to the global confinement scaling, CHS assured the possibility of designing a helical system with a low aspect ratio. It is an important basis in planning a compact helical reactor. Two directions of helical system research for both a high aspect ratio (Ap ~ 10) and a low aspect ratio (Ap ~ 3 - 4) became possible.

The global confinement time of a collisional plasma is better with the standard configuration than the outward shifted one (R_{ax} > 95 cm) even though the plasma volume is smaller than at R_{ax} = 98 cm [9]. This result is opposite to the common understanding of global confinement in relation to MHD stability. In this respect, the magnetic well does not assist better confinement in CHS. On the other hand the global confinement stays on the similar level for the inward shifted configuration (R_{ax} < 92 cm) even though the ideal MHD stability becomes worse. It should be noted that there remains some ambiguity in evaluating the heating efficiency because the behavior of high energy particles are difficult to fully understand both for ECH and NBI heated plasmas. The confinement characteristics of less collisional plasmas will be discussed in Section 6.

A typical electron temperature and density profiles of ECH plasma are shown in Fig. 2. The output power of the 106 GHz gyrotron was 300 kW and the magnetic field was 1.9 T on the magnetic axis in the standard configuration R_{ax} = 92.1 cm. The double folded structure is noticed in the temperature profile. Such structure is general for ECH plasmas in CHS and a much clearer example is obtained for a low density plasma (n_e ~ 2 - 3 $\times 10^{12}$ cm^{-3}) with the electric potential profile measurement by HIBP [10]. The electric potential showed the similar double folded profile. The collisionality of helical ripple trapped particles is less than unity at a half radius in Fig. 2, and the experimentally obtained electron thermal conductivity is close to the neoclassical value (χ_e ~ 3 m^2 sec^{-1}).
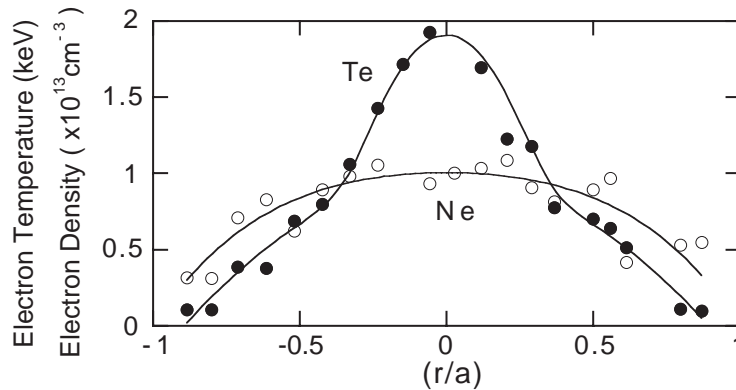

FIG. 2. *Electron temperature and density profiles for 106 GHz ECH heating. R_{ax} = 92.1 cm, B_{axis} = 1.9 T.*

The highest ion temperature was obtained in the high ion temperature mode experiments in CHS using NBI heating [11]. The profile of ion temperature measured by TVCXS diagnostics is shown in Fig. 3 together with the electron temperature and density profiles. The magnetic field was 1.9 T and the configuration with R_{ax} = 92.1 cm was selected. Single co-injection beam was used with a careful tuning for the better beam focusing. Strong wall conditioning with the titanium

gettering was necessary to suppress the wall recycling which resulted in the peaked density profile mostly fueled with the injected beam.
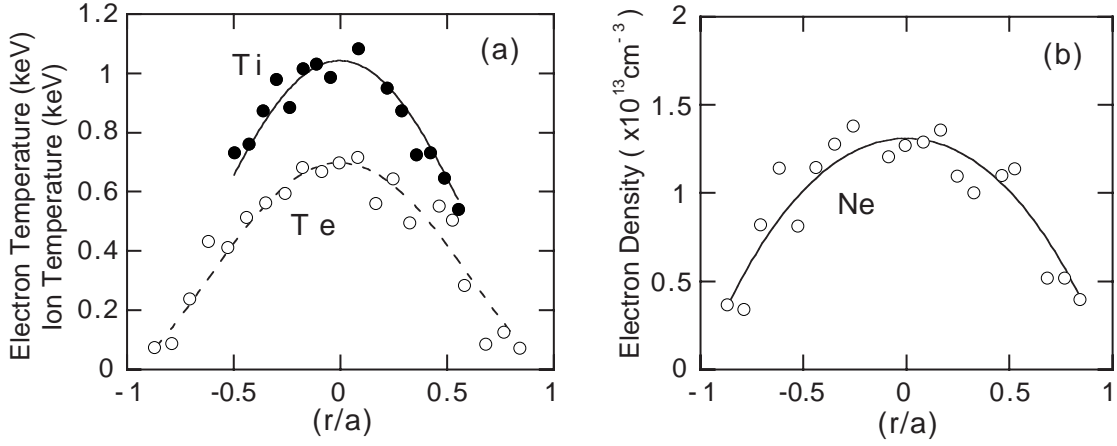

FIG. 3. (a) Ion temperature and electron temperature profiles and (b) electron density profile in high ion temperature mode experiment

CHS has two neutral beam injectors (NBI #1 and #2), the maximum energy of which are 40 keV and 36 keV respectively. Two beams are installed so as to make a balanced tangential injection. One system (NBI #1) is movable to allow various injection angle to the magnetic field for the purpose of high energy particle confinement study. The ratio of the ion Larmor radius to the plasma minor radius is 1/6 to 1/7 for 1 T operation (1/30 for LHD with $E_0 = 180$ keV and $B_t = 3$ T). In the case of tangential injection the toroidal shift of the passing orbit of the beam ions from the magnetic surface becomes 1/2 to 1/3 times minor radius. Combined with large Larmor radius size, the real trajectories of beam ions show very complicated structure especially for the passing boundary particles. As an example, an orbit of a co-injected beam particle with a pitch angel of 48 degree at the detector position is shown in Fig. 4. It makes an excursion out of the LCMS on the outboard side of torus, and comes back into inside of the LCMS.
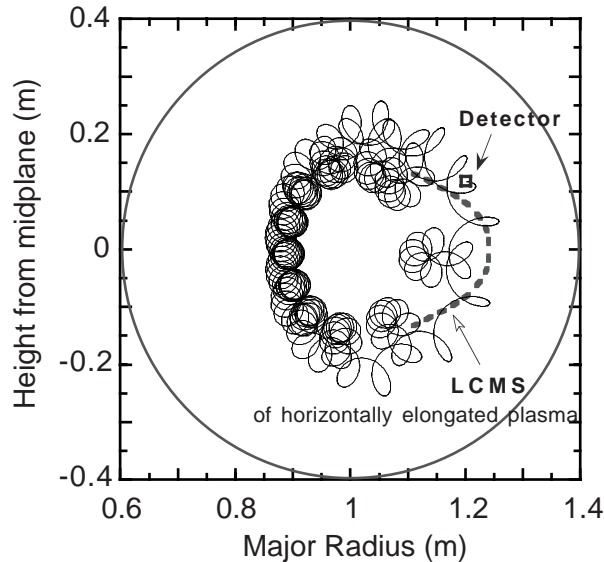

FIG. 4. Toroidal projection of full orbit trajectory for 38 keV proton with 48 degree pitch angle at detector position. The last closed magnetic surface is shown for the toroidal cross section where the escaping particle probe is installed. Magnetic field configuration is $R_{ax} = 94.9$ cm and the magnetic field strength is $B_t = 0.9$ T.

Those particles play an important role not only in the plasma wall interaction, but also in the charge exchange loss of the beam particles. On CHS, an escaping particle probe which resolves the gyro-radius and pitch angle was installed and these particles were studied [12, 13]. Generally, the signal strength of the escaping passing boundary particles shows a similar time evolution to that of plasma pressure.

The pressure of high energy beam ions is large for most of NBI discharges. For low density discharges, total energy of beam components is comparable to the thermal energy of plasmas. Various MHD phenomena are observed which have the close relation to the beam components. Beam driven TAE mode was found in CHS for the first time in helical devices [14], which are closely related to the GAE mode found in Wendelstein 7-AS [15]. Another topic in this field is fishbone like MHD oscillations [14, 16]. This oscillation is observed only for the co-injection of the beam. One possible reason is the difference in the rotational transform profile for the co-injection and the counter-injection. The observed beam driven current was about 10 kA in the experiments with $B_t = 0.9$ T. It can vary the rotational transform considerably (by 30 - 100 %) in the plasma central region which gives large effects on these instabilities.

Toroidal plasma rotation driven by the tangential NBI was studied experimentally and gave an understanding of neoclassical parallel viscosity due to the magnetic field ripples (TTMP effect). The rotation depends largely on the configuration because of the different ripple structures. Figure 5 shows the toroidal plasma rotation speed driven by the co- and counter-beam as a function of R_{ax} [17]. The maximum speed was observed for the configuration with $R_{ax} = 89.9$ cm where the field ripple is minimum as shown in Fig. 1 in Section 1. A more complete calculation of neoclassical parallel viscosity was made based on the magnetic surface averaging of the field gradient $\gamma \ (= < dB/ds >)$ at r/a = 0.2 which is plotted in Fig. 5. The dependence of measured rotation speed on R_{ax} is consistent with this calculated viscosity if the perpendicular viscosity of 0.2 m^2/s is added to slightly modify the profile of rotation. The standard configuration of CHS allows a large toroidal rotation speed which might contribute to better global confinement.
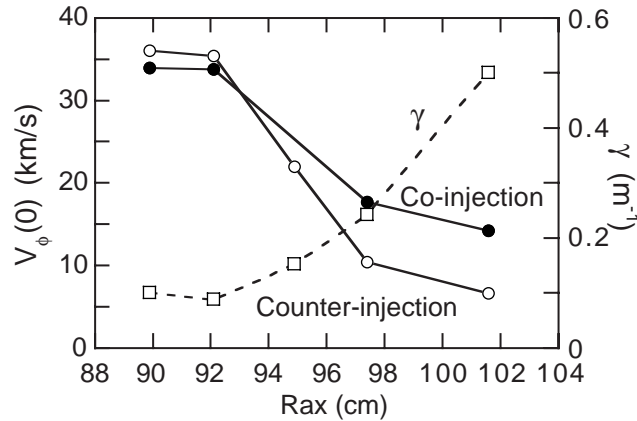

FIG. 5. *Dependence of toroidal rotation velocity of plasma on magnetic axis position. Both co-injection NBI heating and counter-injection case are plotted. Averaged magnetic field gradient γ is also plotted for r/a = 0.2 magnetic surface.*

It was found in the perpendicular beam injection experiments and ICRF heating experiments that the confinement of perpendicular high energy ions is bad in the standard configuration of CHS. In the NBI experiments, NBI #1 which was set for perpendicular injection could not heat the plasma at all [18]. On the other hand, the ICRF experiments were successful in CHS only if the experimental scenario of electron heating was adopted [19]. These results are consistent with the theoretical analysis of trapped particle orbits for the standard configuration.

In order to solve these problems, the experiments were planned to extend the operational range of magnetic axis position R_{ax}. An optimized configuration for the deeply trapped particles is obtained with $R_{ax} = 87.7$ cm. A mod-B minimum contour plot for this configuration is shown in Fig. 6 with a plot for the $R_{ax} = 92.1$ cm as a reference. The plots are made for the magnetic coordinates. To achieve a good coincidence of drift orbits with the magnetic surfaces which are shown in Fig. 6(a), a control of the quadrupole component of the poloidal field is necessary. The toroidally averaged flux surfaces of Fig. 6(a) are almost circular while the standard configuration shown in Fig. 6(b) has a small vertical elongation of the averaged magnetic surfaces.

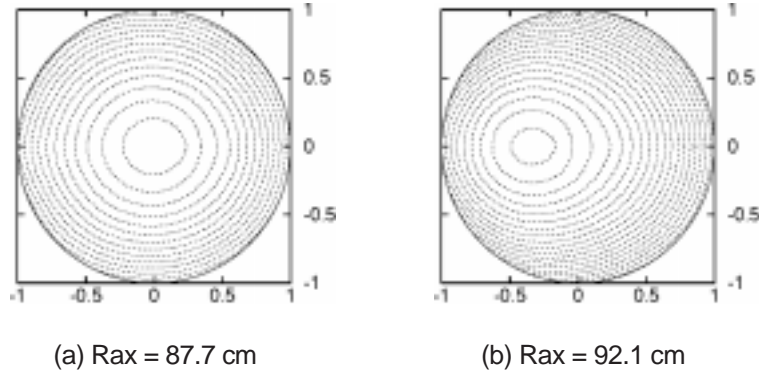

(a) Rax = 87.7 cm   (b) Rax = 92.1 cm

FIG. 6.   Mod-B minimum plots for drift-orbit-optimized configuration $R_{ax} = 87.7$ cm and standard configuration $R_{ax} = 92.1$ cm.

The magnetic field ripple structure for the drift orbit optimized configuration is shown in Fig. 7 for three different minor radii. The minimum values of field strength at all bottoms of ripples are almost constant. Such feature was discussed many years ago in terms of the σ-optimization of the helical magnetic field [20, 21]. More advanced optimization of helical field requires the alignment of the field strength of magnetic field ripples both at their maxima and minima, which is called quasi-omnigenous. It is impossible to make a quasi-omnigenous optimization in CHS based on its existing helical coils. Since the plasma parameters we can obtain in most experiments are barely in the collisionless regime, a partial optimization shown in Fig. 6 and 7 should be effective for improving the confinement.
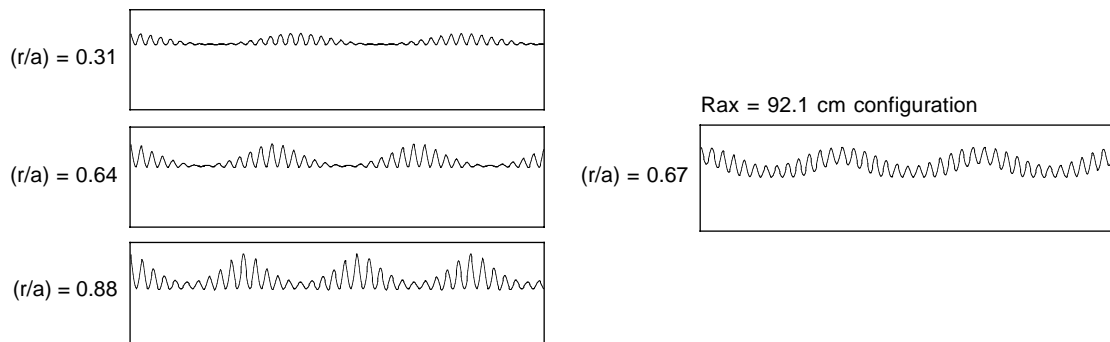

FIG. 7.   Magnetic field ripple structure at three different minor radii for drift-orbit-optimized configuration $R_{ax} = 87.7$ cm. The ripple structure for standard configuration is also plotted for comparison.

4. ELECTRIC FIELD IN THE STANDARD CONFIGURATION

The effect of electric field on the confinement has been discussed in helical systems from the very early phase of its research. It was in the framework of neoclassical transport which is different from the discussion of the effect of electric field shear on the anomalous transport. In helical devices, because the anomalous effect on transport is still large, both aspects of electric field are

important. Large efforts have been made in CHS for the development of diagnostic tools for electric field measurements. The TVCXS measured impurity flow profiles (mostly with carbon impurity) both in the poloidal and toroidal directions and gave information of electric field profiles [22]. This diagnostics worked well for the middle and high density plasmas heated by NBI. The HIBP measured full profiles of electric potential for both ECH and NBI plasmas with a relatively low density [23]. Figure 8 shows the electric field profiles of NBI plasmas measured by TVCXS for three different densities. The magnetic field was about 0.9 T with standard configurations. Stronger electric field was observed for the higher density plasmas. The profile shape and the strength of the electric field is consistent with the neoclassical theory prediction.
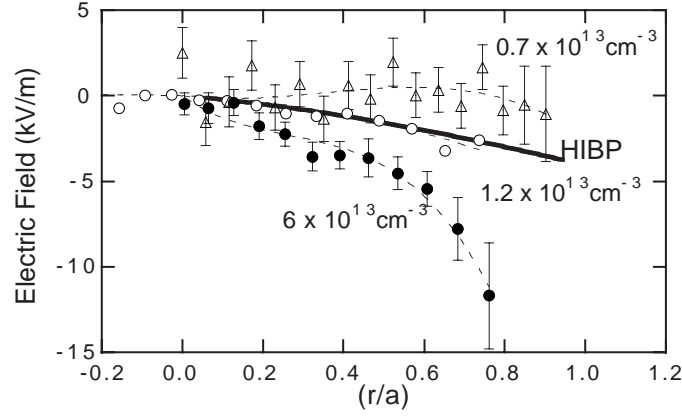

FIG. 8. Electric field measurements by TVCXS diagnostics for NBI plasmas with three different densities. Simultaneous measurement of electric field by HIBP is plotted with a solid line for the middle density case.

The potential profiles for ECH and NBI plasmas measured by HIBP are shown in Fig. 9 for the magnetic field 0.88 T with a standard configuration $R_{ax} = 92.1$ cm. The radial electric field is positive in the central region of ECH plasmas. The potential profile with stronger ECH shows a double folded structure which corresponds to the similar electron temperature profile mentioned in Section 3. The effect of electric field on the neoclassical heat transport has not been clearly identified in the comparison of heat transport coefficient obtained from the experiment with the neoclassical model. The electric field shear at the boundary region of higher density ECH plasma is 50 V/cm^2 which is expected to contribute to the reduction of anomalous transport by about 10 % [10].
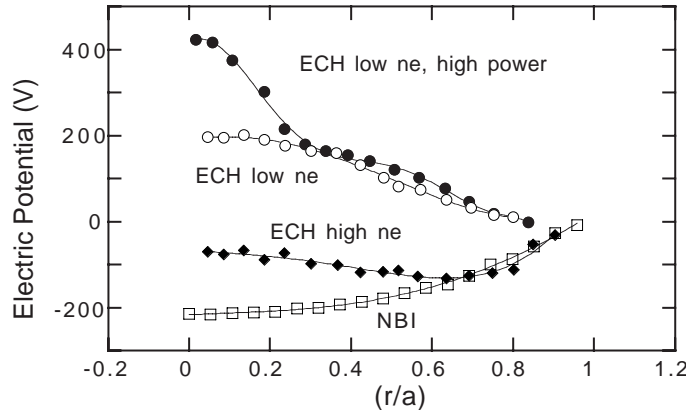

FIG. 9. Electric potential measurements by HIBP diagnostics. Electron densities for low ne ECH was 3×10^{12} cm^{-3}, for high ne ECH, 8×10^{12} cm^{-3}. Input power for high power ECH was 300 kW while others were 100 kW.

HIBP can measure the potential profile of NBI only for the density lower than 2×10^{13}cm^{-3}.

It is because the radiation from the plasma disturbs the measurement of the secondary ionized beam. On the other hand TVCXS has a difficulty in measuring the electric field for low density NBI plasmas because the electric field is very small for these plasmas. Simultaneous measurements of both diagnostics were made successfully for the intermediate density NBI plasma. The solid line in Fig. 8 shows the electric field profile calculated from the potential profile measurement by HIBP for the NBI plasma shown in Fig. 9. The discrete points are plotted from the measurement by TVCXS. These two diagnostics show good agreement with each other for this range of density.

Another effect of electric field on the confinement in helical systems is the resonant loss of high energy trapped particles. Because the radial electric field of NBI plasmas is negative, the $E \times B$ motion and the curvature drift motion are canceled out for a particular energy which causes the direct loss of trapped particles. The energy spectrum of fast neutral particles which have almost perpendicular pitch angles is shown in Fig. 10(a) for the high magnetic field experiment ($B_t = 1.76$ T). It has a dip in the range from 2 to 4 keV. Tail components in the higher energy range come from tangentially injected high energy beam ions. This dip appeared only when strong ion heating occurred. Exponential fitting (shown by the line in the figure) of the perpendicular spectrum in the energy range of $0.45 < E_0 < 1.2$ keV (below the dip energy) gave almost the same ion temperature as the TVCXS gave. Energy spectrum for the measuring angle shifted by 16 degrees (denoted by 'oblique') is also shown in the figure for the comparison. The dip of the spectrum disappeared in this case. Because the spectrum with an intermediate measuring angle showed about 70 % dip compared with the perpendicular case, the width of the resonant loss cone is of the order of 10 degree. The spectrum dip position corresponds to the calculated particle energy for the resonant loss process.
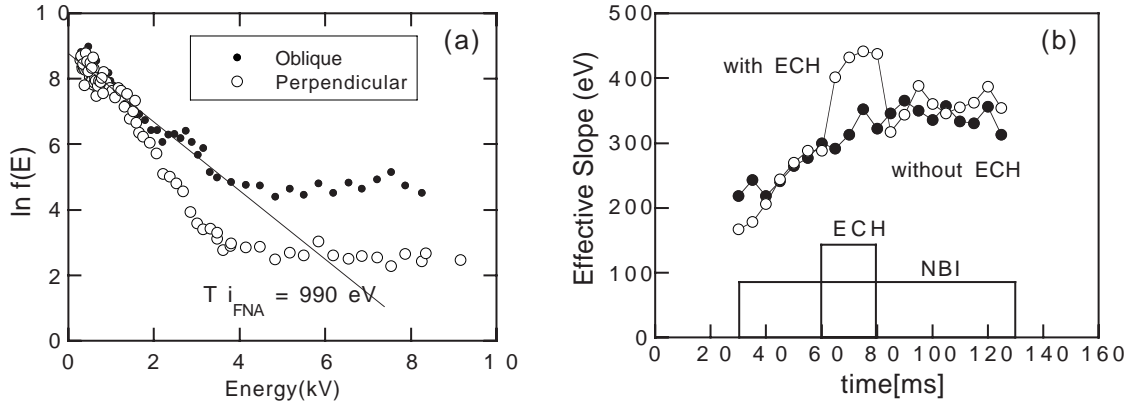

FIG. 10. (a) Spectrum of fast neutral particles obtained by FNA diagnostic. Open circles are from the measurement with perpendicular observation angle to the magnetic field. Small closed circles are with 16 degrees shifted angle. Straight line is the result of spectrum fitting in the energy range : $0.45 < E_0 < 1.2$ keV for getting ion temperature. Magnetic field configuration was $R_{ax} = 92.1$ cm and the field strength was $B_t = 1.76$ T. (b) Time variation of energy spectrum slope in the range of $1 < E_0 < 2$ keV for NBI discharges with and without ECH. The dip of energy spectrum was decreased by application of ECH. The ion temperature measured by TVCXS diagnostic was 600 eV at 70 msec. Magnetic field configuration was $R_{ax} = 92.1$ cm and $B_t = 0.88$ T.

Plasma potential control for NBI plasmas with the application of ECH was demonstrated previously in CHS [24]. The electric field changed from negative to positive during the application of ECH on NBI plasmas. Similar control was made for this plasma by applying 200 kW 53 GHz ECH in the low field experiment ($B_t = 0.88$ T). Time variation of the local slope of the fast neutral particle energy spectrum (explained by an equivalent temperature in the energy range from 1 to 2 keV) is shown in Fig. 10(b) for the perpendicular pitch angle measurement. During ECH, this slope became smaller (higher equivalent temperature) which is the indication of decrease

of the dip in the spectrum. The reduction of the carbon impurity was also observed during ECH pulse. However the ion temperature did not show any significant increase during ECH which indicate that the resonant loss of ions in CHS is still negligible compared with the total energy loss mechanisms of ions.

The electric field has been measured for various discharges in CHS. The profiles are consistent with the neoclassical particle flow modeling for most cases. However the comprehensive evidence of confinement improvement with the electric field has not been obtained so far in CHS because the separation of anomalous loss from the neoclassical transport is difficult for most discharges. Nevertheless some observations were made which showed the coincidence of electric field structure and the temperature profile. One example is high power ECH plasmas which showed a double folded structure both in the potential and temperature profiles. In this case, because the contribution of the central part of a plasma to the total energy is small, an improvement of global confinement is not noticeable. Another example is in the high ion temperature mode experiments which showed the coincidence of transition from L mode to high ion temperature mode with a significant change of electric field profile [11].

5. MHD STABILITY OF OPTIMIZED CONFIGURATION

In discussions of the experimental operation scenarios of Heliotron/Torsatron devices, largely inward shifted configurations are usually excluded because they are (supposed to be) not MHD stable. The ideal interchange stability of Heliotron/Torsatron systems is given by the combination of magnetic well and magnetic shear stabilizing effects. It is a general tendency for all Heliotron/Torsatron devices that the stability is lost when the magnetic surfaces are shifted inward because the magnetic well disappears and the magnetic shear is decreased. It has been discussed that there is no good compatibility of the drift-orbit-optimization and the MHD stability for Heliotron/Torsatron systems.
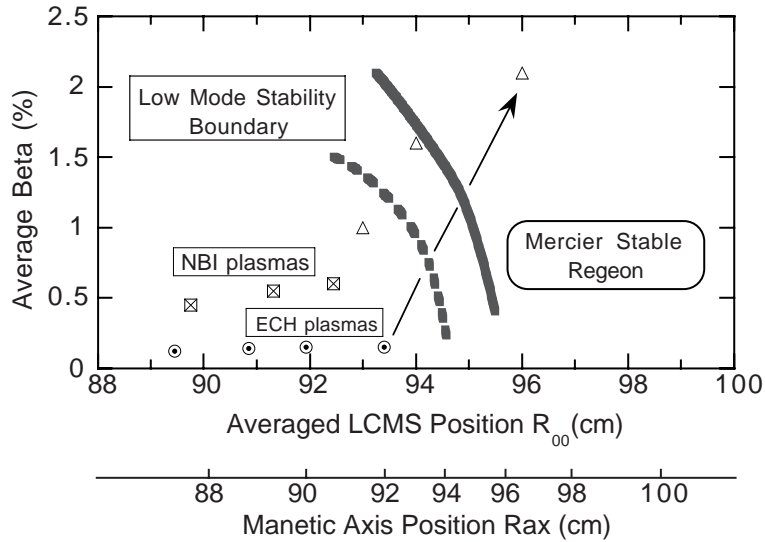

FIG. 11. *Ideal MHD stability map for inward shifted configurations. Solid gray line gives Mercier stability boundary. Dotted one gives low-mode stability boundary. The value R_{ax} is given for the vacuum configuration.*

NBI discharges in CHS appeared to be more stable than the prediction of the ideal interchange stability theory. Discharges in the configurations which have a large Mercier unstable area in the central region were obtained without any instability. Figure 11 shows beta values and the plasma boundary positions of selected discharges from the series of experiments of drift-orbit-optimization. The plasma boundary position R_{00} is defined as an averaged major radius of the last

closed magnetic surface [2]. The R_{ax} parameters for the vacuum cases are shown below the R_{00} values for the comparison between them. Two thick lines in the figure indicate the boundary of the ideal interchange stability from the Mercier criterion. The right side of the solid line (outward shifted configuration) is the region where the equilibrium is Mercier stable for whole plasma region. The equilibrium in the left side has at least one unstable magnetic surface for the interchange mode. Since the low mode instabilities are the most dangerous ones, there is a region of low growth rate of such a mode which is practically stable for the laboratory plasmas even with the Mercier unstable condition. A thick dotted line gives such a low mode stability boundary. The drift-orbit-optimization shown in Fig. 6 is realized at the plasma boundary position $R_{00} = 90$ cm. The square and circle points are the data points with NBI and ECH heating respectively. They are all stable discharges though the Mercier stability analysis predicts instability.

Three triangles in Fig. 11 are taken from the high beta experiments in CHS [4]. An example of the plasma movement is shown by an arrow for the discharge which became Mercier stable as the plasma beta increased (second stability for the interchange mode). The Mercier stability generally becomes better when the plasma beta increases because of the outward shift of the plasma position and the creation of magnetic well due to the Shafranov shift. Fig 11 shows that discharges in the inward shifted configuration of CHS were already stable even before reaching the second Mercier stability. There is a first stability region for very low beta values given by the magnetic shear stabilization effect. But such region is limited for very low beta and is below the beta values of ECH discharges shown in the figure.

The ballooning stability analysis was made for the high beta discharges in Fig. 11 [25]. The calculated stability boundary was close to 2 % beta for strongly localized structure in the toroidal direction. However, since the toroidal Fourier modes for such structure are very high, it is predicted that these modes would not be excited in the real laboratory plasmas. The magnetic fluctuations were measured for various beta values in the experiments. The fluctuation level increased as the beta increased but it was saturated in amplitude when the beta became close to 2 % [26, 16]. Because the fluctuation measurements were made with a poloidal array of magnetic probes which were installed at the toroidal cross section where the ballooning mode is localized, the saturation of magnetic fluctuations at 2 % beta implies that the ballooning mode did not limit the beta. The consideration of power balance including the heating efficiency of NBI could explain the obtained beta value of 2 % [27].

The MHD stability analysis largely depends on the pressure profile of the discharge. Because stabilization due to the magnetic shear works in the boundary region even for the inward shifted configuration, an artificial pressure profile which has a very flat shape in the central region and has a pressure gradient localized only in the boundary region could be Mercier stable. Profiles of temperature and density were measured carefully for all discharges shown in Fig. 11. Two typical examples are shown in Fig. 12 for the standard configuration ($R_{ax} = 92.1$ cm) and for the drift-orbit-optimized configuration ($R_{ax} = 87.7$ cm). No essential difference is found between the two configurations.

In the equilibrium calculation for the stability analysis, the beam pressure profile calculated with a beam deposition code is added to the kinetic pressure. Since the beam pressure in CHS makes up a large part of the total pressure, there remains an ambiguity in the pressure profiles from this part. Total pressure profiles were in the range of normal profiles observed in the CHS experiments which can be described by the formula : $p(r) \propto (1 - r^2)^{\alpha}$ with $1.5 < \alpha < 2.5$. This difference in profile shape does not essentially effect the stability conclusion except for the difference in the ratio of average beta and the central beta values. Difficulty in modeling also comes

---

[2] Plasma position is denoted here by the position of LCMS from the finite beta equilibrium instead of Rax because this parameter is closely related to the MHD stability.

from the large toroidal shift of the passing beam trajectories which causes the non uniformity of the beam pressure on a magnetic surface. Though the contribution of the anisotropic beam pressure to the MHD stability is also important, it usually excites instability (e.g., MHD modes described in Section 3) and it is difficult to find the stabilizing effect given by the beam component.
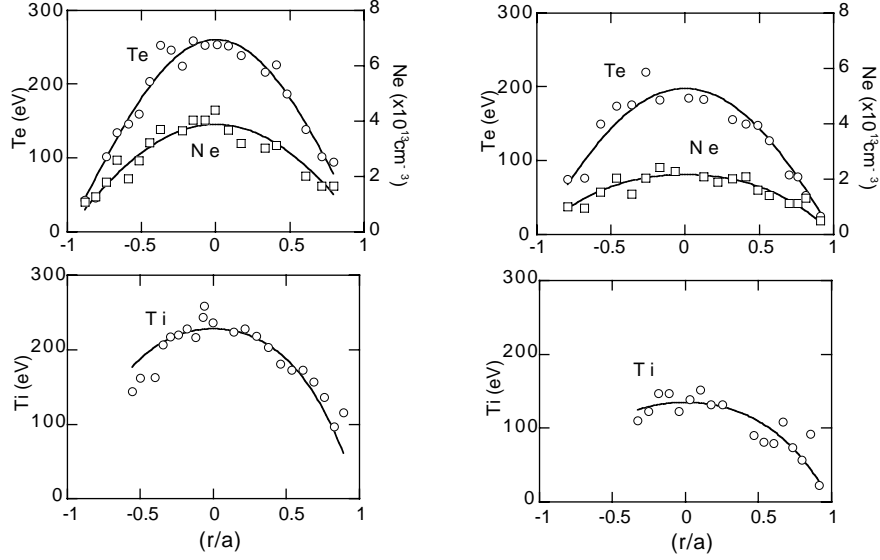

FIG. 12. Plasma temperature and density profiles for standard configuration R_{ax} = 92.1 cm (left side) and R_{ax} = 87.7 cm (right side).
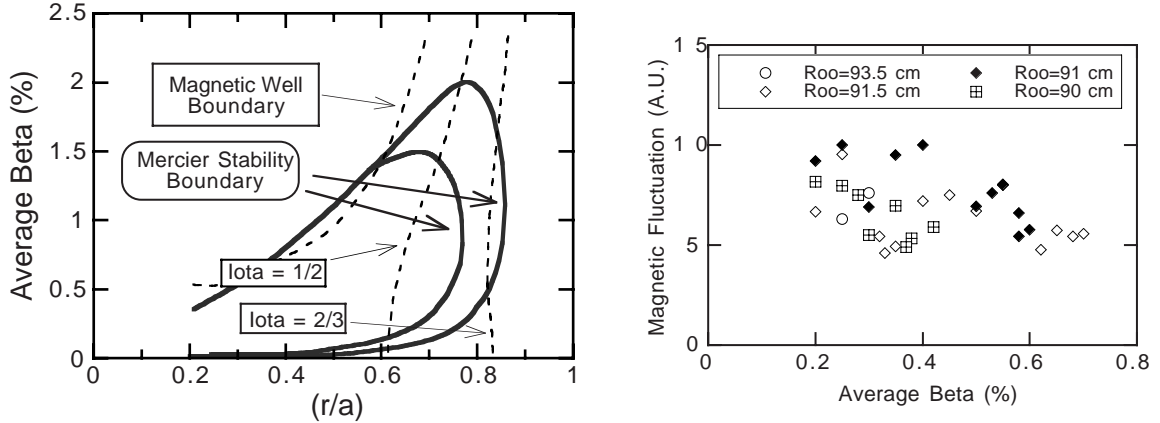

FIG. 13. (left sede) Mercier stability map for R_{ax} = 88.8 cm cofiguration. Contour lines for D_I = 0 (larger area) and D_I = 0.2 (smaller area) are shown. The radius of magnetic well boundary and two low mode rational surfaces are also shown.

FIG. 14. (right side) Dependence of magnetic fluctuations on average beta for different LCMS positions.

The Mercier stability map for the R_{ax} = 88.8 cm is shown in Fig. 13 calculated with the pressure profile : $p(r) \propto (1 - r^2)^2$. The contour lines of a Mercier criterion D_I [28] is plotted for D_I = 0 and D_I = 0.2. Magnetic surfaces inside D_I = 0 contour line for a given beta are unstable for a Mercier criterion. D_I = 0.2 contour line gives the low mode stability boundary [29] which corresponds to the dotted line in Fig. 11. Thin dotted lines are also drawn in Fig. 13 to show the positions of particular radii : the boundary of the magnetic well and the positions of the low order ra-

tional surfaces of 1/2 and 2/3. The magnetic surface with $\iota = 1$ disappears for this inward shifted configuration. Finite beta equilibrium was calculated using the free boundary VMEC code [30] with a vacuum field of the $R_{ax} = 88.8$ cm configuration. Due to the outward shift of the boundary and the Shafranov shift, the equilibrium finally reaches close to the second stability region when the beta reaches 2 %. But the experimental condition shown in Fig. 11 is in an unstable region based on the Mercier criterion.

Figure 14 shows the magnetic fluctuations measured for the NBI discharges shown in Fig. 10 as a function of plasma beta. There are different types of magnetic fluctuations in CHS [14] which were excited either by pressure gradient or by the high energy beam ions. But generally the total fluctuation level is larger for the inward shifted discharges than for the outward shifted ones for $R_{00} > 92$ cm [16]. However for those discharges shown in Fig. 14 ($R_{00} < 92$ cm) they did not increase even though the Mercier stability condition became worse as the plasma position is moved inward.

Beta values achieved for these discharges are lower than the one obtained for the $R_{ax} = 92.1$ cm configuration. It is mostly because the experiment time for the operation of these optimized configuration was not sufficient to achieve as good a machine condition as the high beta experiment campaign with the standard configuration. A reduced plasma volume is also a disadvantageous point for the heating efficiency and also because of the wall effects during the high density operation.

A small disruptive drop of density and energy were observed in discharges with the inward shifted configuration $R_{ax} = 88.8$ cm. But such phenomena could not be observed frequently even when the plasma gets close to the highest obtainable beta value for a particular configuration. There might be hidden parameters for such an instability which have not been clearly understood.

6. CONFINEMENT OF OPTIMIZED CONFIGURATION

The effect of confinement improvement by the drift-orbit-optimization was studied with ECH plasmas with plasma parameters in the low collisionality. Beta values of these plasmas are on the order of 0.1 % and the magnetic field configuration is almost the same as the vacuum configuration. The radial structure of major ripple components are shown in Fig. 15 for the standard configuration ($R_{ax} = 92.1$ cm) and the optimized one ($R_{ax} = 87.7$ cm) in addition to the mod-B minimum contour plots already shown in Fig. 5 in Section 3. A mirror ripple component (poloidal mode is zero) appears in the $R_{ax} = 87.7$ cm configuration although it is very small for $R_{ax} = 92.1$ cm. Because, in central region of the standard configuration, all ripples are considerably small compared to the toroidicity, the transport in the central region is supposed to be dominated by that for an axisymmetric torus. The transport due to helical ripples is important in the region of r/a = 1/3 ~ 2/3. For the region from a half radius to the boundary, the anomalous transport becomes increasingly dominant.

Series of ECH discharges were made for several R_{ax} parameters between the optimized configuration and the standard one. 200 kW of heating power at 53 GHz frequency was used with good microwave beam focusing at the magnetic axis (half width of the gaussian profile for the electric field is 1.5 cm in the poloidal direction). The magnetic field strength on the axis was 0.95 T. The single-path absorption is estimated to be about 70 % for the typical plasma parameters in the experiments. The plasma density was set at $5 - 6 \times 10^{12} \text{cm}^{-3}$ to ensure the collisionless condition.

Figure 16 shows the plasma diamagnetic energy normalized by the plasma volume and the central electron temperature as a function of the position of the magnetic axis R_{ax}. The normalized plasma energy increased as the R_{ax} is shifted inward which demonstrates the confinement im-

provement. But it started to drop before getting to the final optimized configuration $R_{ax} = 87.7$ cm. On the other hand, the increase of the central electron temperature was observed only for $R_{ax} = 91.1$ cm and it decreased for the further inward shift.
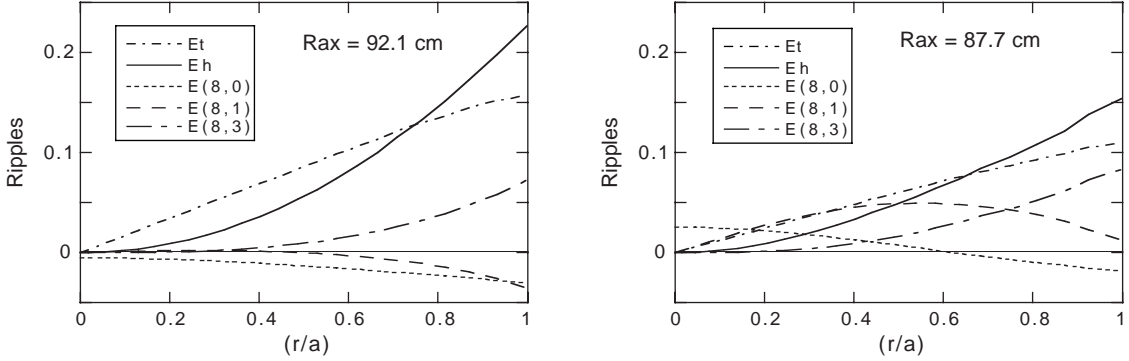

FIG. 15. *Profile of magnetic field ripple structure for standard configuration $R_{ax} = 92.1$ cm and drift-orbit-optiminzed configuration $R_{ax} = 87.7$ cm. Selected components are E_t : toroidicity, E_h : helical ripple (8, 2), mirror ripple (8, 0), side bands (8, 1) and (8, 3).*

Results of the transport analysis for $R_{ax} = 92.1$ cm are shown in Fig. 17. Figure 17a shows the profiles of collisionalities of $\nu_e{}^*$ and $\nu_e{}^{**}$. $\nu_e{}^*$ is the collisionality for the toroidal banana orbit which is the ratio of the electron ion collision frequency ν_{ei} to ν_b, where $\nu_b = \varepsilon_t{}^{3/2} \iota / R$ $(T_e/m_e)^{1/2}$. $\nu_e{}^{**}$ is the collisionality for the helical banana orbit where $\nu_e{}^{**} = \nu_{ei}/\nu_{eq}'$, $\nu_{eq}' = (\varepsilon_h/\varepsilon_t)^{3/4}\nu_b$. Fig 17b shows the calculated neoclassical heat transport coefficients together with the one deduced from the experimental observation of electron temperature profile. Three calculated profiles are shown in Fig. 17b for the transport coefficient which comes from the axisymmetric toroidicity, helical ripples and the sum of these. Since the calculation is based on the single helicity model, the effect of configuration optimization cannot be included.
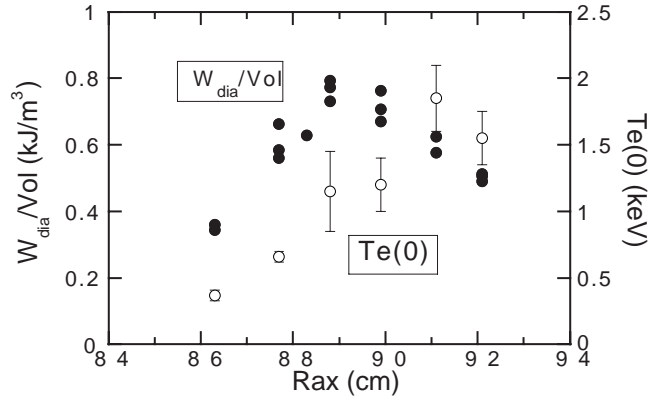

FIG. 16. *Dependence of volume normalized energy and central electron temperature on the position of magnetic axis R_{ax}.*

From this calculation, it is expected that the neoclassical transport in the central region of the $R_{ax} = 92.1$ cm configuration is dominated by the tokamak-like banana particle motions. But in the region near the half radius, transport caused by the helical ripples becomes more important. The increase of the global confinement for the inward shifted configuration comes from the improvement of transport near the half radius because the contribution of this area is much larger than the one from the central region. The configuration optimization had a large effect on the transport in this region by suppressing the ripple diffusion of trapped particles caused by the drift motion. On the other hand, in the central region, the helical ripple diffusion is not the dominating

14

diffusion process for the R_{ax} = 92.1 cm configuration. When the magnetic axis is shifted inward, ripple on the axis is increased as shown in Fig. 1 in Section 2. It is expected that the additional transport appeared due to the increased ripple near the magnetic axis. This might be the reason why the central electron temperature decreased for the inward shifted configuration.
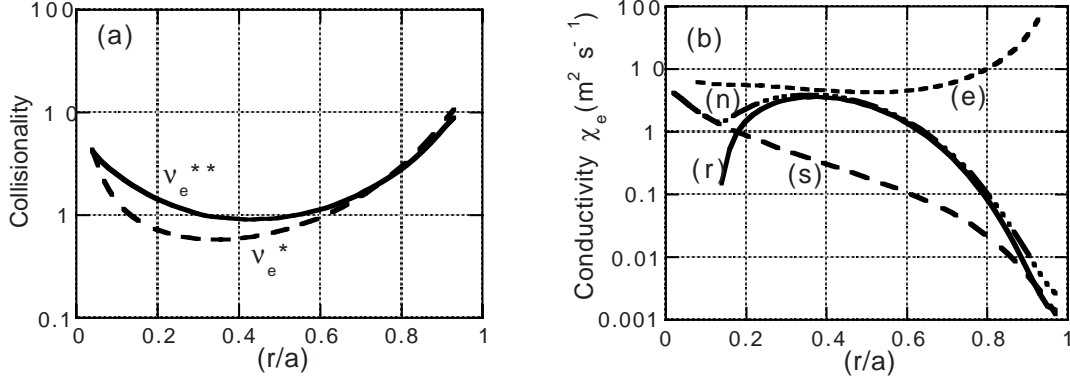

FIG. 17. (a) Collisionality for toroidal banana particles (v_e*) and helical banana particles (v_e**) for ECH plasma shown in standard configuration R_{ax} = 92.1 cm at B_t = 0.88 T. (b) Neo-classical conductivities of tokamak-like symmetric term (s), helical ripple term (r) and sum of these (n) are plotted for the plasma shown in Fig. 16 at R_{ax} = 92.1 cm. Conductivity calculated from the electron temperature profile is plotted as (e). Single helicity model is used. Effect of electric field is not included.

Since the optimized configuration R_{ax} = 87.7 cm is strongly shifted toward the helical coil on the inboard side of torus, a stochasticity of the magnetic surface appears at the boundary with ι = 0.8. It depends also on the quadrupole component. This effect is one of possible causes for the degradation of the global confinement for $R_{ax} < 89$ cm.

The effect of electric field in the neoclassical transport could be another key for understanding the confinement improvement (and the degradation) with the drift-orbit-optimized configuration. The measurement of electric potential for the optimized configuration is planned. The possibility of controlling the mirror ripples on the magnetic axis with additional perturbation coils is also under consideration.

7. CONCLUSION

The Compact Helical System (CHS) experiment has extended the configuration range of helical confinement system to the low-aspect-ratio field. It not only provides necessary scientific support for the continuing new LHD project at NIFS, but also presents a very important achievement for the future direction of helical confinement research on the way to a commercial reactor. The compactness is always the most important key issue.

CHS has developed new advanced diagnostics and fully utilized them to solve fundamental physics problems related to both the general toroidal confinement study and the confinement physics in helical systems. The structures of the electric field and the plasma rotation were investigated in details and quantitatively. Transient phenomena of the potential structure was also revealed. The transport was investigated with an active diagnostic tool using pellet injection. Various kinetic MHD modes were studied which characterize plasmas confined in helical systems.

The improved confinement modes are found for both electron and ion confinement. An internal transport barrier was found for the electron temperature profile which is related to a simi-

lar potential profile. The high ion temperature mode was found for NBI discharges which gave 1 keV ion temperatures.

A wide range of configurations were studied for MHD stability and the confinement improvement. It was found that discharges in Mercier unstable configurations were experimentally stable in CHS. The methods of optimization for Heliotron/Torsatron systems were investigated. The drift-orbit-optimization was tested with low collisionality plasmas and the effect of reduction of helical ripple transport was confirmed. The direction to a more advanced optimization is a future problem.

REFERENCES

[1] MATSUOKA, K., et al., Plasma Physics and Controlled Nuclear Fusion Research 1988 (Proc. 12th Int. Conf. Nice, 1988), Vol. 2, IAEA, Vienna (1989) 411-417.

[2] IIYOSH, A., et al., Fusion Technol. **17** (1990) 169-187.

[3] STROTH, U., et al., Nucl. Fusion **36** (1996) 1063-1077.

[4] OKAMURA, S., et al., Nucl. Fusion **35** (1995) 283-296

[5] FUJISAWA, A., et al., Rev. Sci. Instrum. **63** (1992) 3694-3700.

[6] IDA, K., HIDEKUMA, S., Rev. Sci. Instrum. **60** (1989) 867-871.

[7] SUDO, S., et al., this conference.

[8] TOI, K., et al., Plasma Physics and Controlled Nuclear Fusion Research 1992 (Proc. 14th Int. Conf. Wü rzburg, 1992), Vol. 2, IAEA, Vienna (1993) 461-468.

[9] KANEKO, O., et al., Plasma Physics and Controlled Nuclear Fusion Research 1990 (Proc. 13th Int. Conf. Washington, 1990), Vol. 2, IAEA, Vienna (1991) 473-481.

[10] FUJISAWA, A., et al., Fusion Energy 1996 (Proc. 16th Int. Conf. Montré al, 1996), Vol. 2, IAEA, Vienna (1997) 41-54.

[11] IDA, K., et al., this conference

[12] DARROW, D. S., et al., J. Plasma Fusion Res. SERIES, Vol. 1 (1998) 362-365.

[13] ISOBE, M., et at., to be published in Rev. Sci. Instrum. **70** (1999).

[14] TOI, K., et al., this conference

[15] WELLER, A., et al., Phys. Rev. Lett. **72** (1994) 1220-1223.

[16] SAKAKIBARA, S., et al., J. Phys. Soc. Japan **63** (1994) 4406-4421.

[17] IDA, K., NAKAJIMA, N., Phys. Plasmas **4** (1997) 310-314.

[18] OKAMURA, S., et al., Plasma Physics and Controlled Nuclear Fusion Research 1992 (Proc. 14th Int. Conf. Wü rzburg, 1992), Vol. 2, IAEA, Vienna (1993) 507-514.

[19] MASUDA, S., et al., Nucl. Fusion **37** (1997) 53-68.

[20] MYNICK, H. E., et al., Phys. Rev. Lett. **48** (1982) 322-326.

[21] SHAING, K. C., HOKIN, S. A., Phys. Fluids **26** (1983) 2136-2139.

[22] IDA, K., et al., Phys. Fluids B **3** (1991) 515-518.

[23] FUJISAWA, A., et al., Phys. Plasmas **4** (1997) 1357-1361.

[24] IDEI, H., et al., Phys. Rev. Lett. **71** (1993) 2220-2223.

[25] NAKAJIMA, N., Phys. Plasmas **3** (1996) 4545-4555, 4556-4567.

[26] OKAMURA, S., et al., Plasma Physics and Controlled Nuclear Fusion Research 1994 (Proc. 15th Int. Conf. Seville, 1994), Vol. 1, IAEA, Vienna (1995) 381-388.

[27] MURAKAMI, S., et al., Nucl. Fusion **36** (1996) 359-365.

[28] GLASSER, A. H., GREENE, J. M., JOHNSON, J. L., Phys. Fluids **19** (1976) 567-574.

[29] ICHIGUCHI, K., et al., Nucl. Fusion **33** (1993) 481-492.

[30] HIRSHMAN, S. P., et al., Comput. Phys. Commun. **43** (1986) 143-155.